Biomedicine & Pharmacotherapy 142 (2021) 112034

Contents lists available at ScienceDirect

Biomedicine & Pharmacotherapy

journal homepage: www.elsevier.com/locate/biopha

Tingenone and 22-hydroxytingenone target oxidative stress through downregulation of thioredoxin, leading to DNA double-strand break and JNK/p38-mediated apoptosis in acute myeloid leukemia HL-60 cells

Ana Carolina B. da C. Rodrigues [a], Larissa M. Bomfim [a], Sara P. Neves [a], Milena B.P. Soares [a,b], Rosane B. Dias [a,c], Ludmila F. Valverde [a], Clarissa A. Gurgel Rocha [a,c], Emmanoel V. Costa [d], Felipe M.A. da Silva [d], Waldireny C. Rocha [e], Hector H.F. Koolen [f], Daniel P. Bezerra [a,*]

[a] Gonçalo Moniz Institute, Oswaldo Cruz Foundation (IGM-FIOCRUZ/BA), Salvador, Bahia 40296-710, Brazil
[b] SENAI Institute for Innovation in Advanced Health Systems, SENAI CIMATEC, Salvador, BA 41650-010, Brazil
[c] Department of Clinical Propaedeutics and Integrated Clinical, Faculty of Dentistry, Federal University of Bahia (UFBA), Salvador, Bahia 40301-155, Brazil
[d] Department of Chemistry, Federal University of Amazonas (UFAM), Manaus, Amazonas 69080-900, Brazil
[e] Health and Biotechnology Institute, Federal University of Amazonas (UFAM), Coari, Amazonas 69460-000, Brazil
[f] Metabolomics and Mass Spectrometry Research Group, Amazonas State University (UEA), Manaus, Amazonas 690065-130, Brazil

ARTICLE INFO

Keywords:
Tingenone
22-hydroxytingenone
Thioredoxin
Oxidative stress
Apoptosis
AML

ABSTRACT

Acute myeloid leukemia (AML) is the most lethal form of leukemia. Standard anti-AML treatment remains almost unchanged for decades. Tingenone (TG) and 22-hydroxytingenone (22-HTG) are quinonemethide triterpenes found in the Amazonian plant *Salacia impressifolia* (Celastraceae), with cytotoxic properties in different histological types of cancer cells. In the present work, we investigated the anti-AML action mechanism of TG and 22-HTG in the AML HL-60 cell line. Both compounds exhibited potent cytotoxicity in a panel of cancer cell lines. Mechanistic studies found that TG and 22-HTG reduced cell growth and caused the externalization of phosphatidylserine, the fragmentation of internucleosomal DNA and the loss of mitochondrial transmembrane potential in HL-60 cells. In addition, pre-incubation with Z-VAD(OMe)-FMK, a pan-caspase inhibitor, prevented TG- and 22-HTG-induced apoptosis, indicating cell death by apoptosis via a caspase-dependent pathway. The analysis of the RNA transcripts of several genes indicated the interruption of the cellular antioxidant system, including the downregulation of thioredoxin, as a target for TG and 22-HTG. The application of *N*-acetyl-cysteine, an antioxidant, completely prevented apoptosis induced by TG and 22-HTG, indicating activation of the apoptosis pathway mediated by oxidative stress. Moreover, TG and 22-HTG induced DNA double-strand break and phosphorylation of JNK2 (T183/Y185) and p38α (T180/Y182), and co-incubation with SP 600125 (JNK/SAPK inhibitor) and PD 169316 (p38 MAPK inhibitor) partially prevented apoptosis induced by TG and 22-HTG. Together, these data indicate that TG and 22-HTG are new candidate for anti-AML therapy targeting thioredoxin.

1. Introduction

In 2020, there were an estimated 474,519 new cases and 311,594 deaths from leukemia worldwide [1]. Among the forms of leukemia, acute myeloid leukemia (AML) is the most lethal, and about 19,940 new cases and about 11,180 deaths from AML have been estimated in the United States. The overall ratio of mortality to incidence is 0.56, indicating poor prognosis. The relative 5-year survival rate (2008–2014) is 25% in adults (20 years and over) and 67% in patients aged 0–19 years [2].

Standard anti-AML treatment remains almost unchanged for decades, which includes cytarabine and anthracyclines (daunorubicin or idarubicin). Although most patients achieve high rates of remission, the rate of recurrence is very high [3]. Therefore, new anti-AML drugs are urgently needed.

Tingenone (TG) and 22-hydroxytingenone (22-HTG) (Fig. 1) are quinonemethide triterpenes found in the Amazonian plant *Salacia impressifolia* (Celastraceae). These compounds have been reported as

* Corresponding author.
E-mail address: daniel.bezerra@fiocruz.br (D.P. Bezerra).

https://doi.org/10.1016/j.biopha.2021.112034
Received 28 June 2021; Received in revised form 27 July 2021; Accepted 7 August 2021
Available online 16 August 2021

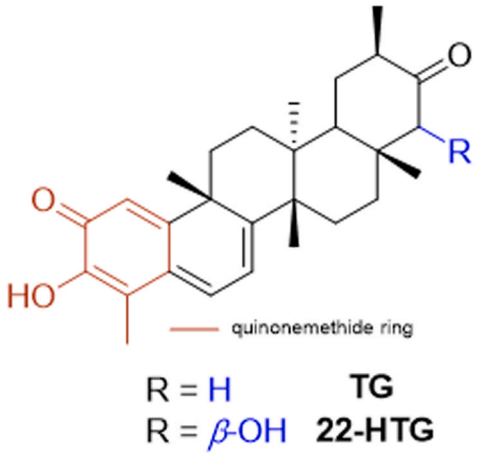

Fig. 1. Chemical structure of TG and 22-HTG.

Table 1
Cytotoxic activity of TG and 22-HTG.

Cells	Histological type	IC_{50} and 95% CI (μM)		
		DOX	TG	22-HTG
Cancer cells				
HL-60	human acute promyelocytic leukemia	0.34 0.23 – 0.48	2.09 1.66 – 2.70	1.58 1.31 – 1.92
Jurkat	human acute T cell leukemia	n.d.	1.50 1.17 – 1.80	1.70 1.05 – 2.68
THP-1	human acute promyelocytic leukemia	0.25 0.16 – 0.44	1.76 1.55 – 2.02	1.26 0.94 – 1.72
KG-1a	human acute myelogenous leukemia	0.18 0.17 – 0.22	3.68 2.83 – 4.83	4.70 3.44 – 6.41
NB4	human acute promyelocytic leukemia	0.46 0.14 – 1.58	0.69 0.17 – 2.66	1.15 0.53 – 2.43
K-562	human chronic myelogenous leukemia	1.53 0.85 – 2.77	2.14 1.83 – 2.52	2.27 1.56 – 3.30
MCF-7	human breast adenocarcinoma	1.51 0.96 – 2.38	5.45 3.66 – 8.06	2.77 1.92 – 4.01
HCT116	human colon carcinoma	0.09 0.05 – 0.16	3.07 2.38 – 3.92	1.21 0.94 – 1.54
HepG2	human hepatocellular carcinoma	0.32 0.18 – 0.55	8.58 6.40– 11.58	2.31 1.51 – 3.55
CAL 27	human tongue squamous cell carcinoma	0.34 1.65 – 0.69	1.66 1.12 – 2.45	1.26 0.89 – 1.76
HSC-3	human tongue squamous cell carcinoma	0.53 0.39 – 0.73	2.07 1.31 – 3.21	1.56 1.08 – 2.29
SCC-4	human tongue squamous cell carcinoma	2.1 1.7–2.6	1.02 0.74 – 1.38	1.15 0.92 – 1.44
B16-F10	mouse melanoma	0.15 0.07 – 0.18	2.26 1.62 – 3.16	1.97 1.33 – 2.93
Non-cancerous cells				
MRC-5	human lung fibroblast	1.65 1.03 – 2.61	2.83 2.26 – 3.57	2.82 2.36 – 3.37
BJ	human foreskin fibroblast	3.60 1.15 – 11.22	3.28 2.23 – 4.83	2.57 1.33 – 3.67
PBMC	human peripheral blood mononuclear cells	1.21 0.73 – 1.99	0.81 0.62 – 1.05	n.d.

cytotoxic agents in different histological types of cancer cells [4–9]. In particular, 22-HTG induced apoptosis and suppressed invasion of melanoma cells by inhibiting the activity of metalloproteinases (MMP-2 and MMP-9) and the expression of the BRAF, NRAS and KRAS genes [7,8]. TG and 22-HTG inhibited tubulin polymerization in vitro [9] and TG has also been identified through in silico study as a pro-apoptotic agent [10]. However, the mechanism of action of these compounds is not yet known. In the present work, we investigated the anti-AML action mechanism of TG and 22-HTG in the AML HL-60 cell line.

2. Material and methods

2.1. Tingenone and 22-hydroxytingenone obtaining

TG and 22-HTG were isolated from the stem bark of *S. impressifolia* using different chromatographic techniques, as previously described [6]. For all experiments, TG and 22-HTG were dissolved in sterile dimethyl sulfoxide (DMSO, Vetec Química Fina Ltda, Duque de Caxias, RJ, Brazil) at a 5 mg/mL stock solution and diluted with culture medium at different concentrations.

2.2. Cells

A total of 13 cancer cell lines, 3 non-cancer cells and 1 mutant and its parent cell line were used in this study and details can be found in Table S1. The American Type Culture Collection (ATCC, Manassas, VA, USA) animal cell culture guide was used for all cell line procedures and mycoplasma test was carried out using a mycoplasma stain kit (Sigma-Aldrich Co., Saint Louis, MO, USA) to validate the use of mycoplasma-free cells. Cells were cultured in RPMI-1640 medium (Gibco-BRL, Gaithersburg, MD, USA) or DMEN-F12 medium (Gibco-BRL) with 10% (or 20% for KG-1a) fetal bovine serum (Life, Carlsbad, CA, USA) and 50 μg/mL of gentamicin (Life, Carlsbad, CA, USA). Trypsin-EDTA solution (Gibco-BRL) was used to collect adherent cells. All cell lines were grown in flasks at 37 °C in 5% CO_2 and subcultured every 3–4 days to maintain exponential growth. All experiments were carried out at exponential growth phase.

2.3. Alamar blue assay

Cell viability was quantified by Alamar blue assay, as previously described [11–13]. The cells were plated in 96-well culture plates (3×10^4 cells/well for suspension cells and 7×10^3 cells/well for adherent cells) and kept at 37 °C and 5% CO_2 atmosphere. The compounds (0.19–25 μg/mL) were added to each well and incubated for 72 h. Doxorubicin (0.04–5 μg/mL) (purity ≥ 95%, doxorubicin hydrochloride, Laboratory IMA S.A.I.C., Buenos Aires, Argentina) was used as a positive control. Four (for cell lines) or 24 h (for PBMCs) before the end of incubation, 20 μL of a stock solution (0.312 mg/mL) of resazurin (Sigma-Aldrich Co.) was added to each well. Absorbances at 570 nm and 600 nm were measured using a SpectraMax 190 Microplate Reader (Molecular Devices, Sunnyvale, CA, USA). Experiments was conducted three times independently.

For subsequent experiments, HL-60 cells (3×10^5/mL) were seeded in 24-well plate and treated with TG (0.6 and 1.2 μM) and 22-HTG (1.2 and 2.4 μM) for 24 and/or 48 h. The negative control was treated with the vehicle (0.2% DMSO) that was used to solubilize and dilute the triterpenes, and doxorubicin (1 μM) was used as a positive control.

2.4. Trypan blue exclusion assay

After the treatment time, cells were removed from the suspension and added to the trypan blue (0.4%) solution (1:10 dilution). Cells that excluded trypan blue were counted as viable and cells stained in blue, due to membrane damage, were considered non-viable. Cell counting was carried out in a hemocytometer using a light microscope.

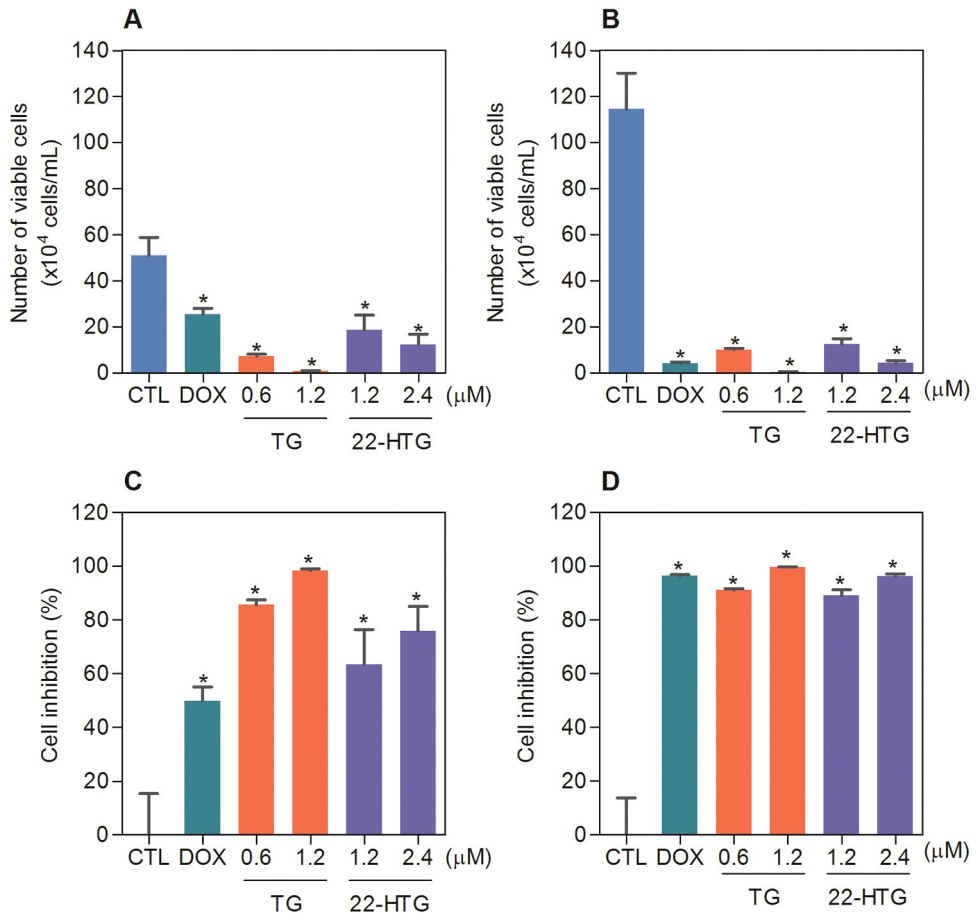

Fig. 2. Trypan blue exclusion assay after 24 (A and C) and 48 (B and D) h of treatment with TG and 22-HTG. The vehicle (0.2% DMSO) was used as a negative control (CTL) and doxorubicin (DOX, 1 μM) was used as a positive control. Data are shown as mean ± S.E.M. of three independent experiments carried out in duplicate. *$p < 0.05$ compared with CTL by ANOVA followed by Student Newman-Keuls test.

Experiments was conducted three times independently.

2.5. Internucleosomal DNA fragmentation and cell cycle distribution

Internucleosomal DNA fragmentation and cell cycle distribution were quantified through DNA content, as previously described [14]. In this assay, HL-60 cells were removed from the plate, washed with PBS and harvested in a permeabilization solution containing 0.1% Triton X-100, 2 μg/mL propidium iodide (PI), 0.1% sodium citrate and 100 μg/mL RNAse (all from Sigma-Aldrich Co.), and incubated in the dark at room temperature for 15 min. Cell fluorescence was quantified by flow cytometry. For all flow cytometry analyses, at least 10.000 events/sample were acquired using a BD LSRFortessa cytometer along with BD FACSDiva Software (BD Biosciences, San Jose, CA, EUA) and Flowjo Software 10 (Flowjo LCC, Ashland, OR, USA). Cell debris were excluded from the analysis. Experiments was conducted three times independently.

2.6. Morphological analysis

To evaluate alterations in the morphology, 150 μL of each sample was centrifuged on slides in a cytospin at 2000 rpm for 10 min. Cell fixation was performed with methanol for 1 min, then the slides with a monolayer of cells were stained with hematoxylin and eosin. Morphological alterations were observed and photographed by light microscopy (Leica Microsystems, Wetzlar, Germany). Light scattering features were obtained by flow cytometry, as described above.

2.7. Apoptosis detection

Apoptosis detection was performed using FITC Annexin V Apoptosis Detection Kit I (ID 556547) (BD Biosciences), according to the manufacturer's instructions. HL-60 cells were gently harvested from the plate, washed with PBS, resuspended in binding buffer, and incubated with Annexin V-FITC and PI at room temperature for 15 min. The cell fluorescence was determined by flow cytometry, as described above. Functional assays using pan-caspase inhibitor (Z-VAD(Ome)-FMK, Cayman Chemical; Ann Arbor, MI, USA), antioxidant (*N*-acetyl-cysteine, NAC, Sigma-Aldrich), p38 MAPK inhibitor (PD 169316; Cayman Chemical), JNK/SAPK inhibitor (SP 600125; Cayman Chemical) and MEK inhibitor (U-0126; Cayman Chemical) were also performed. For that, cells were pre-incubated for 2 h with 50 μM Z-VAD(Ome)-FMK, 5 mM NAC, 5 μM PD 169316, 5 μM SP 600125 and 5 μM U-0126, followed by incubation with 1.2 μM TG and 2.4 μM 22- HTG for 48 h. Experiments was conducted three times independently.

2.8. Mitochondrial transmembrane potential

To assess mitochondrial transmembrane potential loss, HL-60 cells were washed twice with PBS, then incubated with rhodamine 123 (5 μg/mL, Sigma-Aldrich Co.) at 37 °C for 15 min in the dark and resuspended with PBS. The mitochondrial transmembrane potential was performed by retention of dye rhodamine 123, as described previously [15]. The cell fluorescence was determined by flow cytometry, as described above. Experiments was conducted three times independently.

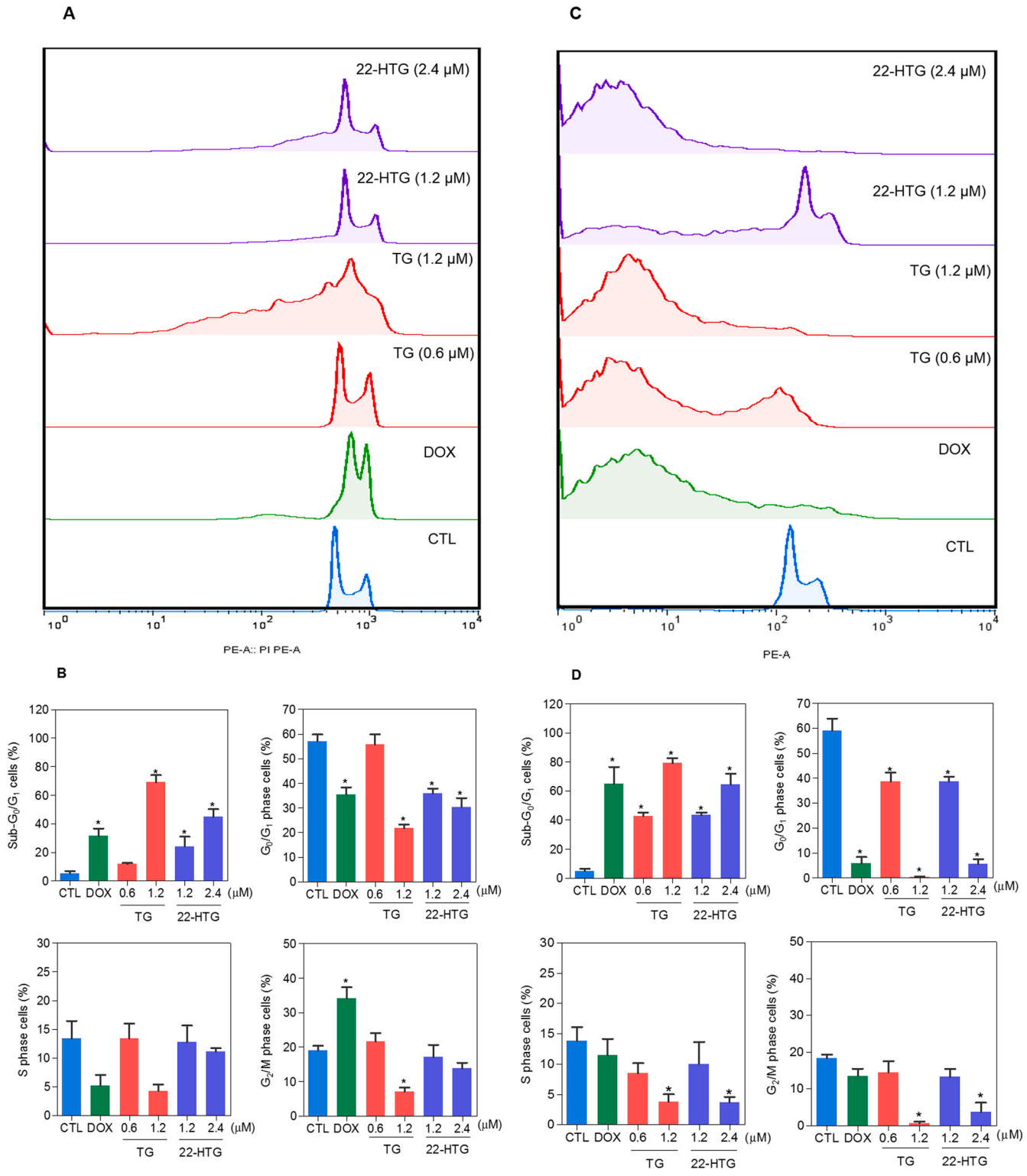

Fig. 3. Cell cycle distribution of HL-60 cells after 24 (A and B) and 48 (C and D) h of incubation with TG and 22-HTG. The vehicle (0.2% DMSO) was used as a negative control (CTL) and doxorubicin (DOX, 1 μM) was used as a positive control. Data are shown as mean ± S.E.M. of three independent experiments carried out in duplicate. *$p < 0.05$ compared with CTL by ANOVA followed by Student Newman-Keuls test.

2.9. RT-qPCR array

HL-60 cells were incubated with 1.2 μM TG or 2.4 μM 22-HTG for 12 h and total RNA was isolated from the cells using the RNeasy Plus Mini Kit (Qiagen; Hilden, Germany), according to the manufacturer's instructions. The RNA was analyzed for purity and quantified by a NanoDrop® 1000 spectrophotometer (Thermo Fisher Scientific, Waltham, Massachusetts, USA). RNA reverse transcription was carried out using a Superscript VILO™ Kit (Invitrogen Corporation; Waltham, MA, USA). TaqMan® array human cancer drug targets 96-well plate, fast (ID RPRWENH, Applied Biosystems™, Foster City, CA, USA) was used for the gene expression study by qPCR. The reactions were conducted in an

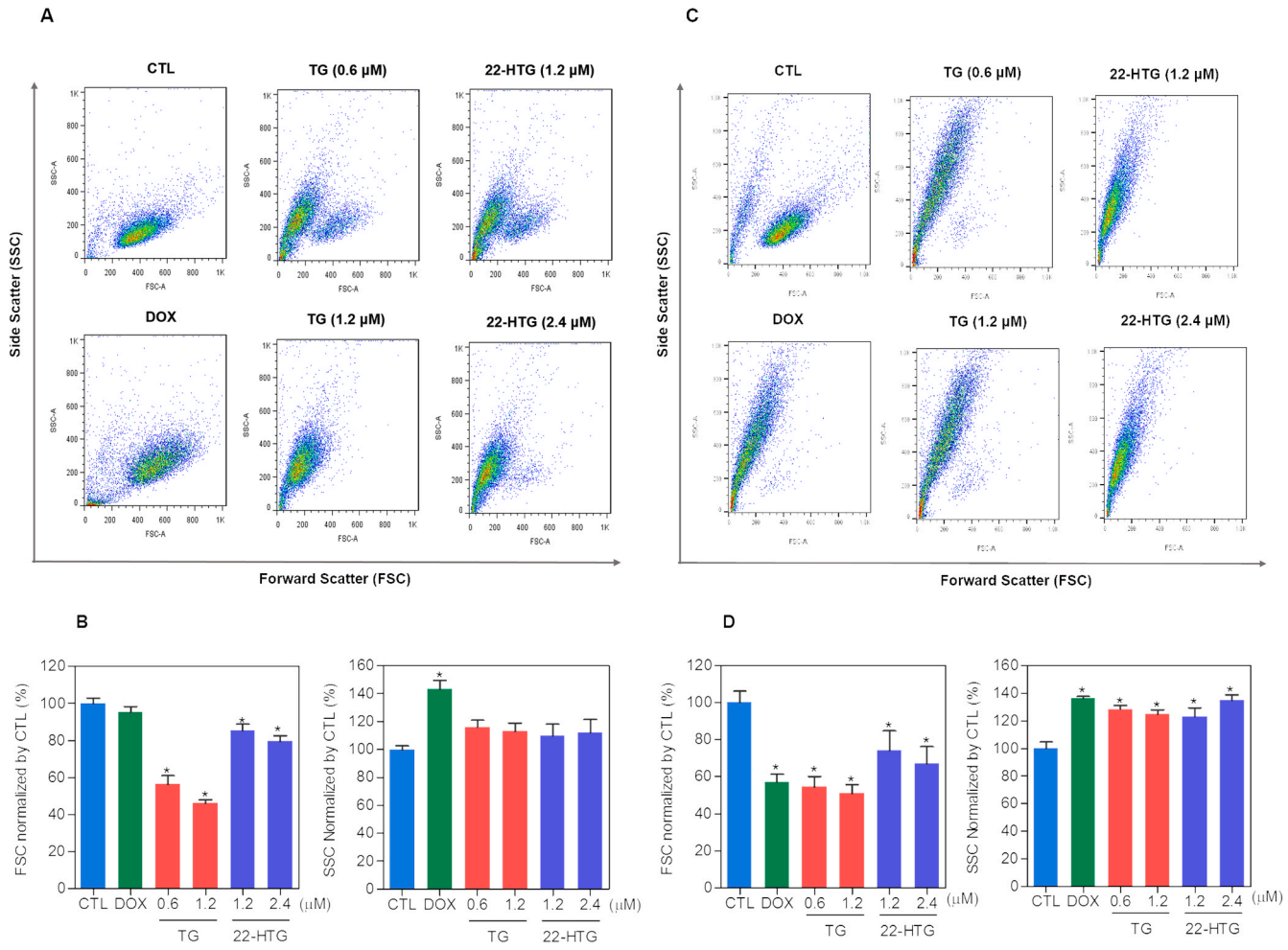

Fig. 4. Light scattering features of HL-60 cells after 24 (A and B) and 48 (C and D) h of treatment with TG and 22-HTG. The vehicle (0.2% DMSO) was used as a negative control (CTL) and doxorubicin (DOX, 1 μM) was used as a positive control. Data are shown as mean ± S.E.M. of three independent experiments carried out in duplicate. *$p < 0.05$ compared with CTL by ANOVA followed by Student Newman-Keuls test.

ABI ViiA7 system (Applied Biosystems™). The cycle conditions comprised 2 min at 50 °C, 10 min at 95 °C, then 40 cycles of 15 s at 95 °C and 1 min at 60 °C. The relative quantification (RQ) of mRNA expression was calculated by the $2^{-\Delta\Delta CT}$ method [16] using Gene Expression Suite™ Software (Applied Biosystems™), and the cells treated with the negative control (0.2% DMSO) were used as a calibrator. The reactions were normalized by the geometric mean of the RQ of the reference genes GAPDH, HPRT1, PGK1 and RLPL0. All experiments were performed in DNase/RNase-free conditions. The genes were considered to be upregulated if the RQ≥ 2, which means that the gene expression in TG- and 22-HTG-treated cells were at least twice that of the negative control-treated cells. Similarly, the genes were considered to be downregulated if RQ ≤ 0.5, which means that the gene expression in TG- and 22-HTG-treated cells were at least half of that of the negative control-treated cells.

2.10. Phospho-specific ELISA

Phosphorylated histone H2AX (S139) (ID DYC2288-2), JNK2 (T183/Y185) (ID DYC2236-2), p38α (T180/Y182) (DYC869B-2) and ERK1 (T202/Y204) (ID DYC1825-2) expression levels were measured in cell lysates using sandwich ELISA kits (all from R&D Systems, Inc. Minneapolis, MN, USA), according to the manufacturer's instructions. HL-60 cells were seeded in a 24–well plate and incubated following treatment with 1.2 μM TG or 2.4 μM 22-HTG for 15 min, 30 min or 24 h, then cells were harvested and suspended in lysis buffer plus phosphatase and protease inhibitors cocktail and 1 mM PMSF (all from Sigma-Aldrich Co.). Total protein quantification was carried out in each sample by Pierce Protein Assay (Thermo Fisher Scientific, Waltham, MA, USA) using BSA as standard. Absorbance at 450 nm was measured using a SpectraMax 190 Microplate Reader (Molecular Devices, Sunnyvale, CA, USA). Experiments was conducted three times independently.

2.11. DNA interaction assay

DNA interaction was measured in a cell-free system using calf thymus DNA (ctDNA, Sigma-Aldrich Co.), as previously described [17]. The reaction mixture containing 15 μg/mL ctDNA, 1.5 μM ethidium bromide (Sigma-Aldrich Co.) and TG (5 and 10 μM) or 22-HTG (5 and 10 μM) in 100 μL of 0.9% NaCl solution were added to 96-well plates. The vehicle (0.2% DMSO) was used as negative control and doxorubicin (10 μM) was used as positive control. Fluorescence was measured using the excitation and emission wavelengths of 320 and 600 nm, respectively, using a Spectramax Microplate Reader (Molecular Devices).

2.12. Statistical analysis

Data were presented as mean ± S.E.M. or as IC_{50} values with 95% confidence intervals obtained by nonlinear regressions. The differences between the experimental groups were compared through analysis of variance (ANOVA) followed by Student–Newman–Keuls test ($p < 0.05$). All statistical analyzes were performed using the GraphPad Prism

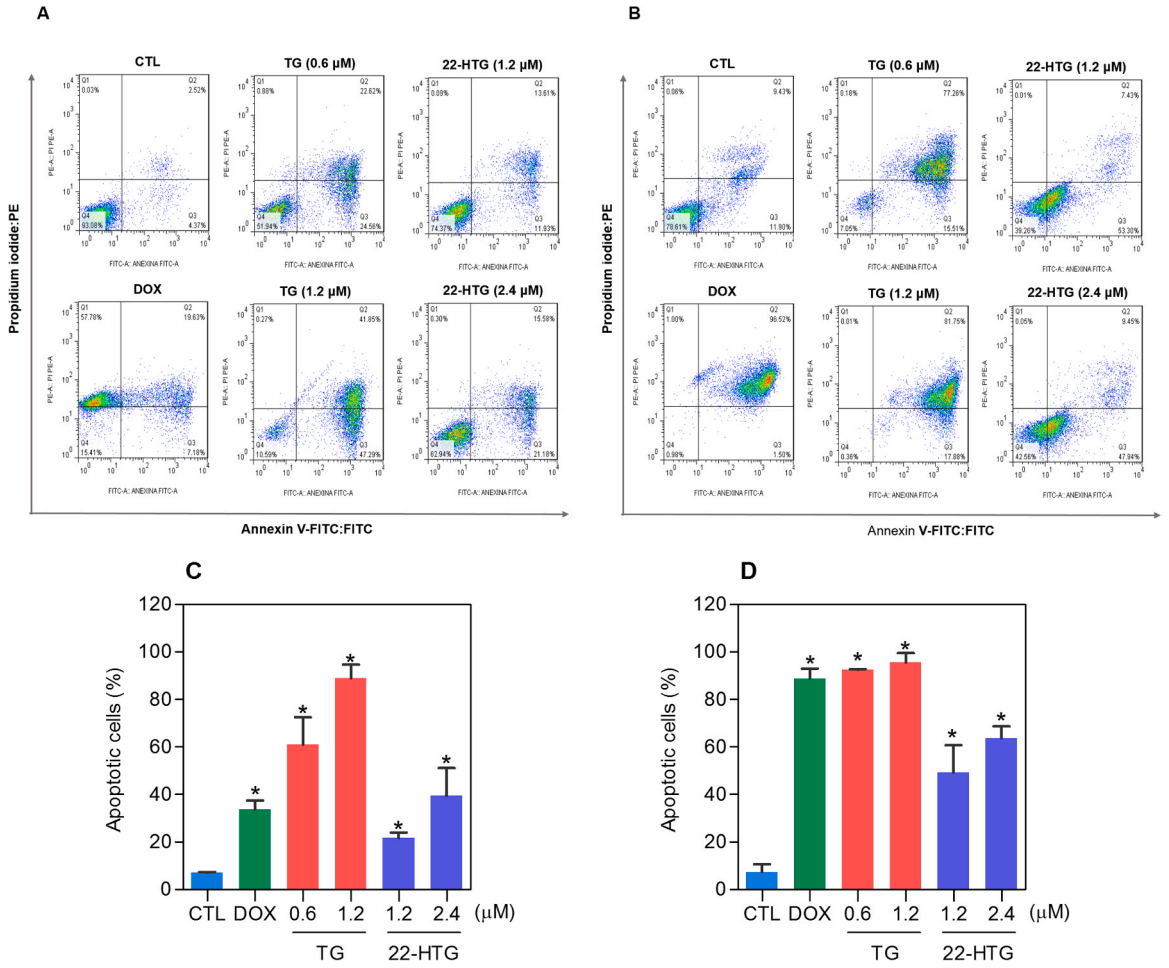

Fig. 5. Induction of apoptosis in HL-60 cells after 24 (A and C) and 48 (B and D) h of treatment with TG and 22-HTG. (A and B) Representative flow cytometric dot plots. (C and D) Quantification of apoptotic HL-60 cells (annexin V-FITC positive cells). The vehicle (0.2% DMSO) was used as a negative control (CTL) and doxorubicin (DOX, 1 μM) was used as a positive control. Data are shown as mean ± S.E.M. of three independent experiments carried out in duplicate. *$p < 0.05$ compared with CTL by ANOVA followed by Student Newman-Keuls test.

(Intuitive Software for Science; San Diego, CA, USA).

3. Results

3.1. Tingenone and 22-hydroxytingenone present potent cytotoxicity in a panel of cancer cells

The cytotoxicity of TG and 22-HTG was evaluated in a panel of 13 different cancer cell lines and 3 non-cancerous cells through the Alamar blue assay after 72 h of incubation. Table 1 shows the data obtained. TG showed IC_{50} values that ranged from 0.69 to 8.58 μM for the cancer cell lines NB4 and HepG2, respectively, while 22-HTG showed IC_{50} values that ranged from 1.15 to 4.70 μM for the cancer cell lines NB4/SCC4 and KG-1a, respectively. Doxorubicin was used as a positive control and showed IC_{50} values ranging from 0.09 to 1.53 μM for the cancer cell lines HCT116 and K562, respectively. Table S2 presents the selectivity index calculated. These data indicated low selectivity of TG and 22-HTG. Doxorubicin also showed potent cytotoxicity to non-cancerous cells.

These data were calculated by nonlinear regression from three independent experiments carried out in duplicate, as quantified by alamar blue assay after 72 h. Doxorubicin (DOX) was used as a positive control. n.d. = not determined.

Next, cell viability was assessed after 24 and 48 h of incubation with TG and 22-HTG with the trypan blue exclusion assay in HL-60 cells (Fig. 2). At concentrations of 0.6 and 1.2 μM, TG reduced the number of viable cells by 85.7% and 98.4% after 24 h and 91.2% and 99.7% after 48 h, respectively. At concentrations of 1.2 and 2.4 μM, 22-HTG reduced the number of viable cells by 63.5% and 76.0% after 24 h and 89.1% and 96.2% after 48 h, respectively. Doxorubicin (1 μM) decreased the number of viable cells by 50.0% and 96.4% after 24 and 48 h of incubation, respectively.

3.2. Tingenone and 22-hydroxytingenone induce caspase-mediated apoptotic cell death in HL-60 cells

In a new set of experiments, DNA content was measured by flow cytometry to quantify the internucleosomal DNA fragmentation and cell cycle distribution in TG- and 22-HTG-treated HL-60 cells (Fig. 3). DNA that was subdiploid (sub-G_0/G_1) was considered fragmented. Both compounds induced DNA fragmentation ($p < 0.05$). At concentrations of 0.6 and 1.2 μM, TG increased the percentage of cells with DNA fragmentation by 12.0% and 69.0% after 24 h and 43.0% and 79.2% after 48 h, respectively. At concentrations of 1.2 and 2.4 μM, 22-HTG increased the percentage of cells with DNA fragmentation by 24.13% and 44.88% after 24 h and 43.5% and 64.5% after 48 h, respectively. Doxorubicin induced cell cycle arrest in G_2/M phase, followed by DNA fragmentation.

Cell morphology was evaluated by light microscopy using hematoxylin & eosin staining after 48 h of treatment (Fig. S1). TG and 22-HTG caused chromatin condensation, cell shrinkage and fragmentation of the nuclei. These morphological features were also observed by flow cytometry through light-scattering where both compounds caused cell

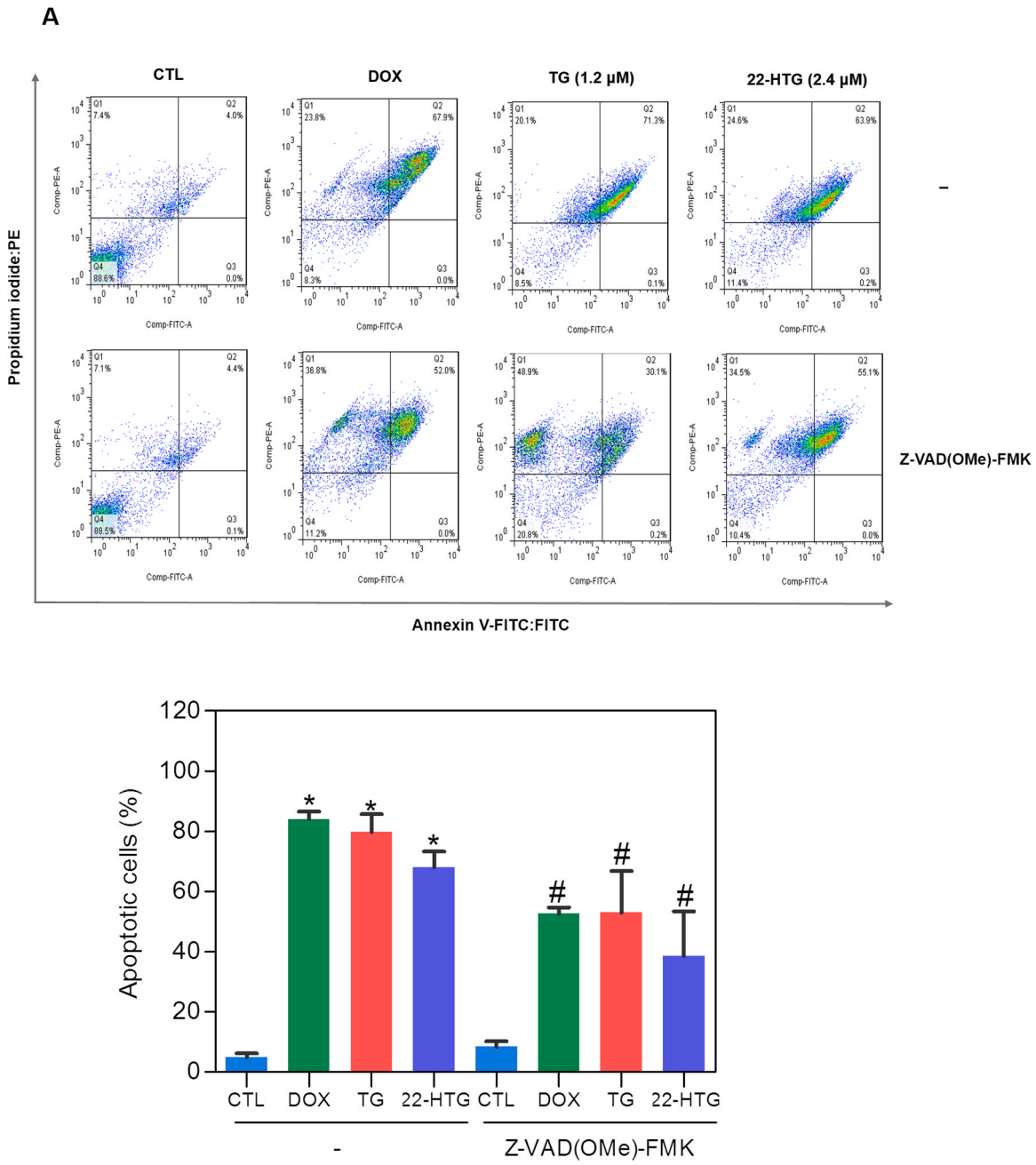

Fig. 6. Action of a pan-caspase inhibitor (Z-VAD(OMe)-FMK) in the apoptosis caused by TG and 22-HTG in HL-60 cells. (A) Representative flow cytometric dot plots. (B) Quantification of apoptotic HL-60 cells (annexin V-FITC positive cells). The cells were pre-treated for 2 h with 50 μM Z-VAD(OMe)-FMK, then incubated with TG at 1.2 μM or 22-HTG at 2.4 μM for 48 h. The vehicle (0.2% DMSO) was used as a negative control (CTL) and doxorubicin (DOX, 1 μM) was used as a positive control. Data are shown as mean ± S.E.M. of three independent experiments carried out in duplicate. *$p < 0.05$ compared with CTL by ANOVA followed by Student Newman-Keuls test. # $p < 0.05$ compared with the respective treatment without inhibitor by ANOVA followed by Student Newman-Keuls test.

shrinkage, as observed by the decrease in forward-light scatter, and nuclear condensation, as observed by the increase in side scatter (Fig. 4). These morphological chances are associated with apoptotic cell death. Interestingly, doxorubicin also induced morphological changes associated with apoptosis.

Next, annexin V-FITC, a Ca^{2+}-dependent protein with affinity for phosphatidylserine, was used to quantify phosphatidylserine externalization, as an apoptosis marker, and the dye PI was used to assess the loss of membrane integrity, as a necrosis marker. The cells were measured through annexin-V-FITC/PI double staining using flow cytometry after 24 and 48 h. Therefore, viable (those cells that were negative for annexin-V-FITC and PI), early apoptotic (those cells that were positive for annexin-V- FITC, but negative for PI), late apoptotic cells (those cells that were positive for annexin- V-FITC and PI) and necrotic (annexin-V-FITC negative and PI positive) cells were quantified. Both complexes significantly increased the percentage of apoptotic cells (all cells that were positive for annexin-V-FITC) (Fig. 5). At concentrations of 0.6 and 1.2 μM, TG increased the percentage of apoptotic cells by 60.9% and 88.8% after 24 h and 92.4% and 95.5% after 48 h, respectively. At concentrations of 1.2 and 2.4 μM, 22-HTG increased the percentage of apoptotic cells by 21.7% and 39.5% after 24 h and 49.2% and 63.7% after 48 h, respectively. Doxorubicin (1 μM) also increased the percentage of apoptotic cells by 33.6% and 88.8% after 24 and 48 h, respectively.

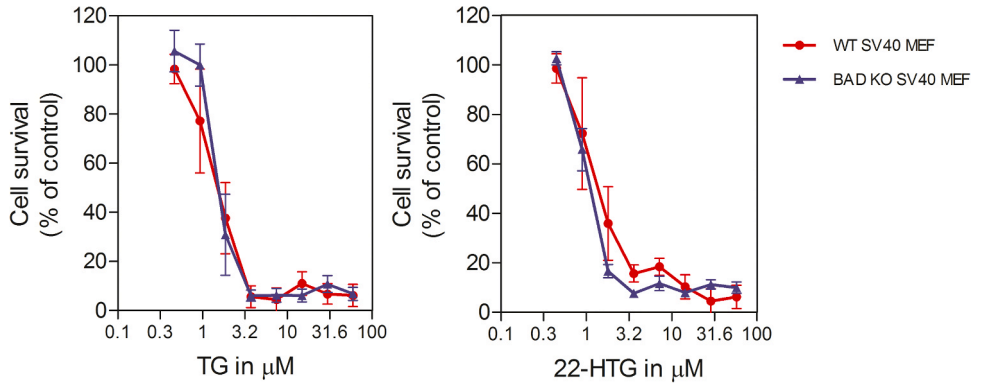

Fig. 7. Survival curves of BAD KO SV40 MEF and WT SV40 MEF cell lines upon treatment with TG and 22-HTG. The curves were obtained from at least three independent experiments carried out in duplicate using Alamar blue assay after 72 h of treatment.

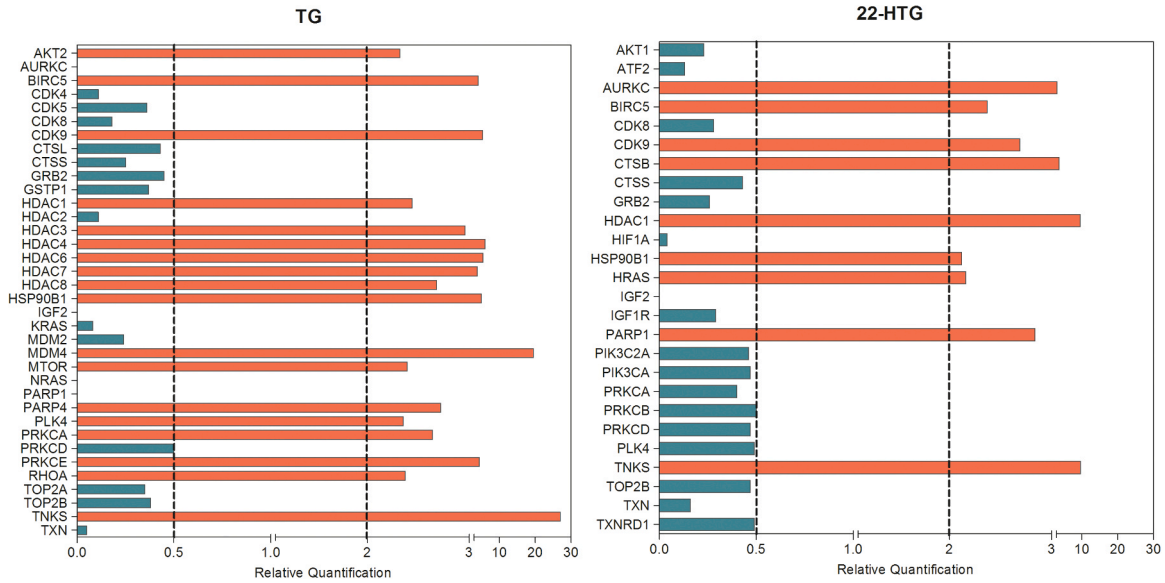

Fig. 8. Genes up- and down-regulated in HL-60 cells after 12 h of treatment with 1.2 μM of TG or 2.4 μM of 22-HTG. The negative control was treated with the vehicle (0.2% DMSO). Values represent the relative quantification (RQ) compared with the calibrator (cells treated with the negative control). The genes were considered to be upregulated if RQ $\geq$ 2 (red bars) and were considered to be downregulated if RQ $\leq$ 0.5 (green bars).

To evaluate the role of caspases in the apoptosis induced by TG and 22-HTG, Z-VAD(OMe)-FMK, a pan-caspase inhibitor, was used. Interestingly, co-treatment with Z-VAD(OMe)-FMK partly decreased the apoptosis induced by TG and 22-HTG (Fig. 6), indicating apoptosis mediated by caspases. The mitochondrial transmembrane potential was also decreased in TG- and 22-HTG-treated cells (Fig. S2).

In additional experiments, we examined the role of BAD gene in the cell death induced by TG and 22-HTG using BAD KO SV40 MEF cell line and in its parental WT SV40 MEF cell line (Fig. 7). The effect of TG and 22-HTG on cell viability was similar in BAD KO SV40 MEF and WT SV40 MEF cell lines, indicating that the BAD gene is not essential for their cytotoxicity.

3.3. Tingenone and 22-hydroxytingenone target oxidative stress through downregulation of thioredoxin leading apoptosis in HL-60 cells

To understand the mechanism of action, the effects of TG and 22-HTG on the expression of 82 genes related to apoptosis, PI3 kinases & phosphatases, growth factors & receptors, drug metabolism, G-protein signaling, hormone receptors, heat shock proteins, receptor tyrosine kinase signaling, cathepsins, cell cycle, topoisomerases type II, transcription factors, protein kinases, RAS signaling, histone deacetylases, poly ADP-ribose polymerases and structural proteins were detected after 12 h of incubation on HL-60 cells by RT-qPCR array using TaqMan® array human cancer drug targets 96-well plate.

A total of 18 and 9 upregulated genes and 18 and 17 downregulated genes were identified after treatment with TG and 22-HTG, respectively (Fig. 8 and Table S3). Among them, TG downregulated the growth factor gene IGF2, the drug metabolism gene GSTP1 and TXN, the cell cycle genes CDK4, CDK5 and CDK8, the topoisomerases genes TOP2A and TOP2B, the protein kinase gene AURKC, the RAS signaling genes HRAS, KRAS and NRAS, and the poly ADP-ribose polymerase gene PARP1. While downregulation of the growth factor gene IGF2 and its related receptor IGF1R, the drug metabolism genes TXN and TXNRD1, the cell cycle gene CDK8, the topoisomerases gene TOP2B, the transcription factors genes ATF2 and HIF1A, and protein kinases genes PLK4, PRKCA, PRKCB, PRKCC and PRKCD were found after treatment with 22-HTG. Curiously, the gene belongs to the cellular antioxidant system thioredoxin (TXN) was negatively modulated by TG and 22-HTG. Moreover, TG also downregulated the gene expression of glutathione S-transferase pi 1 (GSTP1) and 22-HTG downregulated the gene expression of thioredoxin reductase 1 (TXNRD1) that are important antioxidant enzymes that can protect cells from oxidative stress in various human cancers. These data indicate that the interruption of the cellular antioxidant

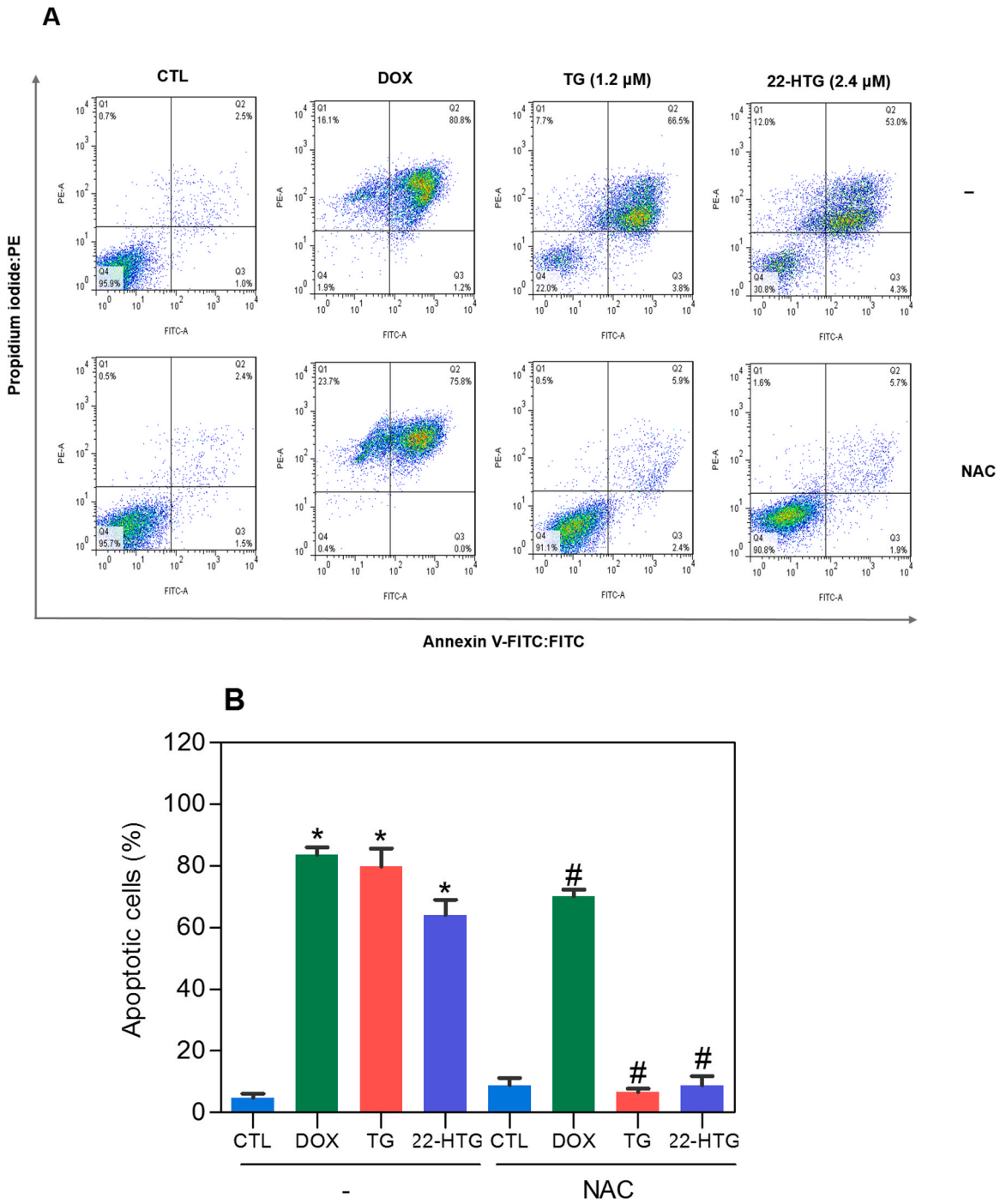

Fig. 9. Action of the antioxidant *N*-acetyl-cysteine (NAC) in the apoptosis induced by TG and 22-HTG in HL-60 cells. (A) Representative flow cytometric dot plots. (B) Quantification of apoptotic HL-60 cells (annexin V-FITC positive cells). The cells were pre-treated for 2 h with 5 mM NAC, and then incubated with TG at 1.2 µM or 22-HTG at 2.4 µM for 48 h. The vehicle (0.2% DMSO) was used as a negative control (CTL) and doxorubicin (DOX, 1 µM) was used as a positive control. Data are shown as mean ± S.E.M. of three independent experiments carried out in duplicate. *$p < 0.05$ compared with CTL by ANOVA followed by Student Newman-Keuls test. # $p < 0.05$ compared with the respective treatment without inhibitor by ANOVA followed by Student Newman-Keuls test.

system, including downregulation of thioredoxin, as a target of TG and 22-HTG.

Based on the fact of TG and 22-HTG can downregulate the cellular antioxidant system, we decided to study the role of oxidative stress in the cell death induced by these compounds. For that, we measured the apoptotic cells induced by TG and 22-HTG in HL-60 cells that were co-treated with the antioxidant NAC. Interestingly, NAC completely inhibited TG- and 22-HTG-induced apoptosis in HL-60 cells (Fig. 9), indicating that these compounds induce oxidative stress-mediated apoptotic cell death.

3.4. Tingenone and 22-hydroxytingenone cause DNA damage in HL-60 cells

Induction of oxidative stress can lead to DNA damage. Therefore, we decide to assess DNA double-strand break in HL-60 cells treated with TG and 22-HTG. Phospho-histone H2AX (S139) (also called γH2AX), a DNA double-strand break marker, expression was measured after 24 h of

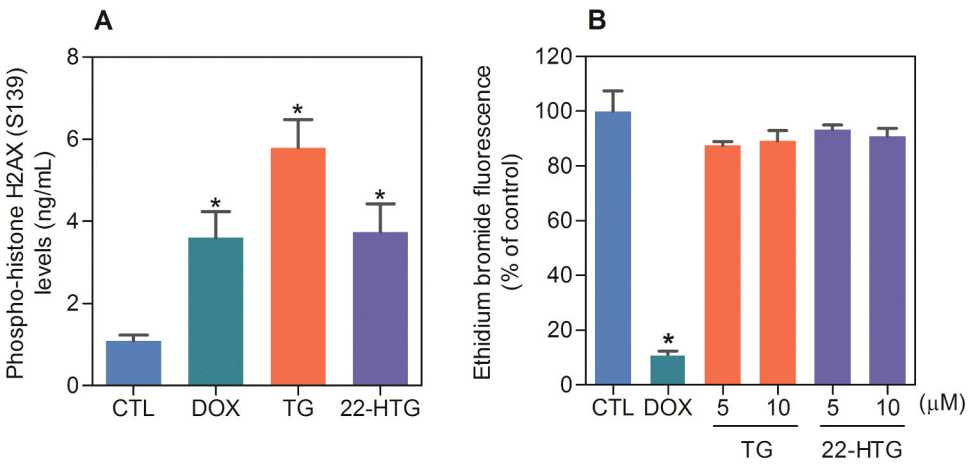

Fig. 10. (A) Phospho-histone H2AX (S139) expression level in HL-60 cells treated with TG at 1.2 μM and 22-HTG at 2.4 μM for 24 h. (B) DNA interaction ability of TG and 22-HTG using ethidium bromide replacement method in a cell-free system with calf thymus DNA. The vehicle (0.2% DMSO) was used as a negative control (CTL) and doxorubicin (DOX, 1 μM) was used as a positive control. Data are shown as mean ± S.E.M. of three independent experiments carried out in duplicate. $^{*}p < 0.05$ compared with CTL by ANOVA followed by Student Newman-Keuls test.

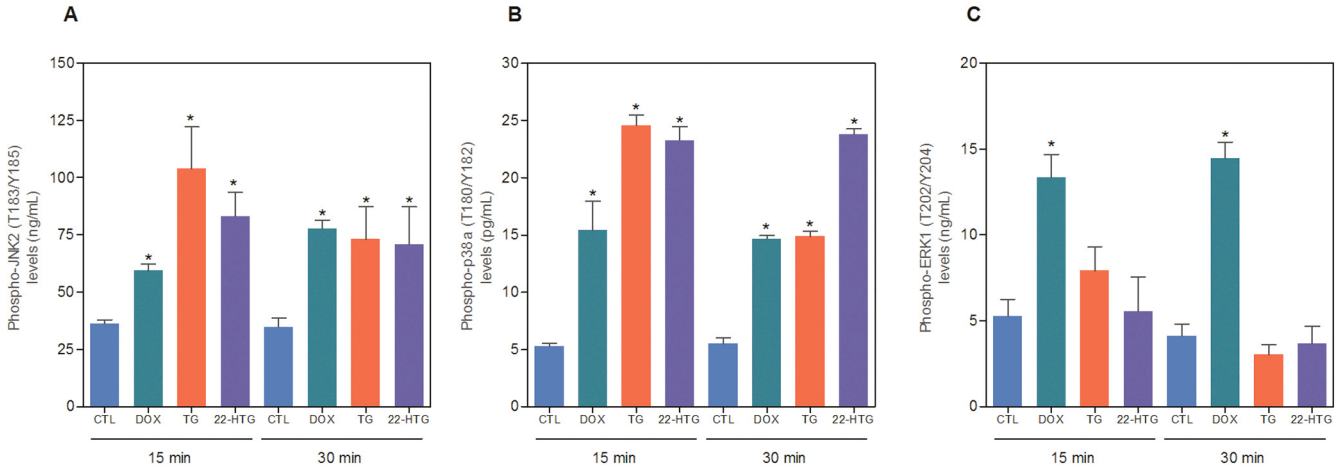

Fig. 11. Phospho-JNK2 (T183/Y185), phospho-p38α (T180/Y182) and phospho-ERK1 (T202/Y204) expression levels in HL-60 cells treated with TG at 1.2 μM or 22-HTG at 2.4 μM. (A) Quantification of phospho-JNK2 (T183/Y185) expression. (B) Quantification of phospho-p38α (T180/Y182) expression. (C) Quantification of phospho-ERK1 (T202/Y204) expression. The vehicle (0.2% DMSO) was used as a negative control (CTL) and doxorubicin (DOX, 1 μM) was used as a positive control. Data are shown as mean ± S.E.M. of three independent experiments carried out in duplicate. $^{*}p < 0.05$ compared with CTL by ANOVA followed by Student Newman-Keuls test.

incubation. Interestingly, treatment with both compounds induced an augment of phosphorylation of histone H2AX (S139), indicating DNA damage (Fig. 10A).

To evaluate whether the DNA damage is caused by a direct DNA-binding ability, TG and 22-HTG were evaluated in a cell-free system using a ctDNA model by ethidium bromide replacement method. In this model, the ability of drugs to displace the ethidium bromide-DNA complex and subsequently reduce the fluorescence is measured. At 5 and 10 μM, neither TG nor 22-HTG significantly decreased the fluorescence intensity, indicating that DNA is not a primary target to these compounds (Fig. 10B). Doxorubicin (10 μM), a known drug that intercalate with DNA, was used as a positive control and decreased the fluorescence intensity by 89.0%.

3.5. Tingenone and 22-hydroxytingenone cause JNK/p38-mediated apoptosis in HL-60 cells

Since mitogen-activated protein kinase (MAPK) signaling is involved in oxidative stress-mediated apoptosis, we decided to evaluate the participation of the MAPK pathway in the apoptosis caused by TG and 22-HTG in HL-60 cells. For that, the levels of expression of phospho-JNK2 (T183/Y185), phospho-p38α (T180/Y182) and phospho-ERK1 (T202/Y204) were also measured after 15 and 30 min of treatment. Moreover, the apoptotic cell death caused by TG and 22-HTG was also quantified in HL-60 cells co-incubated with MAPK inhibitors. Interestingly, treatment with TG and 22-HTG increased the phosphorylation of JNK2 (T183/Y185) and phospho-p38α (T180/Y182), without change phospho-ERK1 (T202/Y204) expression levels (Fig. 11). In addition, co-incubation with a JNK/SAPK inhibitor (SP 600125) and a p38 MAPK inhibitor (PD 169316), but not a MEK (mitogen-activated protein kinase kinase) inhibitor (U-0126) that inhibits the activation of ERK1/2, prevent partially TG and 22-HTG-induced apoptosis, indicating apoptotic cell death through JNK/p38 pathways in HL-60 cells (Fig. 12).

4. Discussion

Herein, we demonstrated that TG and 22-HTG target oxidative stress through downregulation of thioredoxin leading DNA damage and MAPK-mediated apoptosis in AML cell line HL-60. This is the first report on the ability of TG and 22-HTG to inhibit the cellular antioxidant system, including downregulation of thioredoxin, as a target of their cytotoxicity.

Metabolic reprogramming is known as a hallmark of cancer. In this context, aberrant metabolism leads to increased oxidative stress in cancer cells [18]. Interestingly, thioredoxin reductase 1 has been reported to be overexpressed in several types of cancer, including

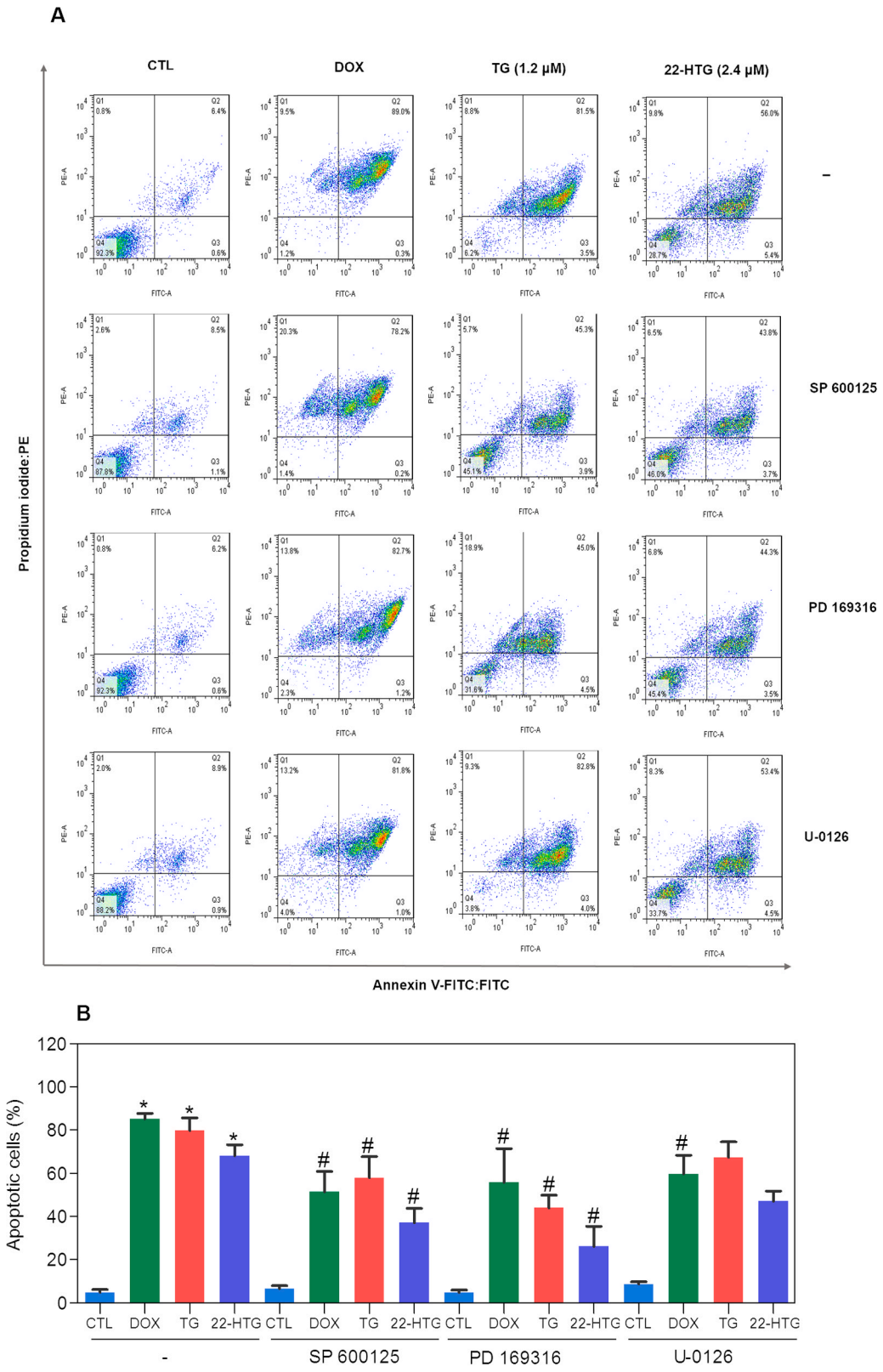

Fig. 12. Action of the JNK/SAPK inhibitor (SP 600125), p38 MAPK inhibitor (PD 169316) and MEK inhibitor (U-0126) on the apoptosis induced by TG and 22-HTG in HL-60 cells. (A) Representative flow cytometric dot plots. (B) Quantification of apoptotic HL-60 cells (annexin V-FITC positive cells). Cells were pretreated for 2 h with 5 μM U-0126, 5 μM SP 600125 or 5 μM PD 169316 and then incubated with TG at 1.2 μM or 22-HTG at 2.4 μM for 48 h. The vehicle (0.2% DMSO) was used as a negative control (CTL) and doxorubicin (DOX, 1 μM) was used as a positive control. Data are shown as mean ± S.E.M. of three independent experiments carried out in duplicate. *$p < 0.05$ compared with CTL by ANOVA followed by Student Newman-Keuls test. # $P < 0.05$ compared with the respective treatment without inhibitor by ANOVA, followed by the Student-Newman-Keuls test.

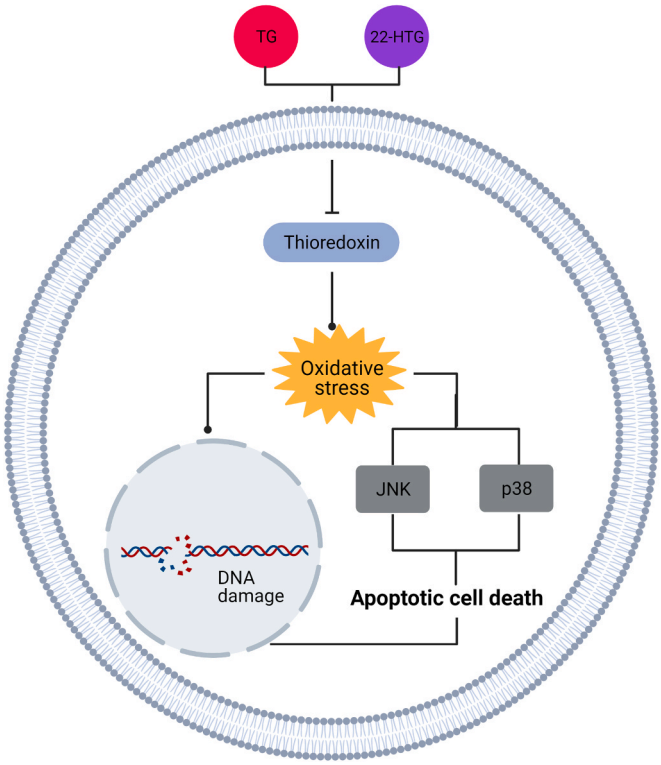

Fig. 13. Molecular mechanism of action proposed for TG and 22-HTG in HL-60 cells.

leukemia. The thioredoxin system is an important class of the mammalian antioxidant system, which scavenges reactive oxygen species to maintain intracellular redox homeostasis. It is composed by thioredoxin, thioredoxin reductase and nicotinamide adenine dinucleotide phosphate (NADPH) [19–24]. Moreover, thioredoxin knockdown with shRNA inhibits the growth of prostate cancer cells [25].

Using a RT-qPCR array, we identified downregulation of thioredoxin as target of TG and 22-HTG. In addition, 22-HTG also downregulated the gene expression of thioredoxin reductase 1. Likewise, TG also downregulated the gene expression of glutathione S-transferase pi 1, another important regulator of oxidative stress, acting by combining glutathione with electrophiles [26]. Furthermore, by functional assay using the antioxidant NAC, we observed that TG and 22-HTG induce oxidative stress-mediated apoptotic cell death.

Pristimerin, a quinonemethide triterpene structurally related to TG and 22-HTG, has been previously reported to inhibit thioredoxin, leading to apoptosis and autophagy through activation of ROS/ASK1/JNK pathway in human breast cancer [27]. Moreover, pristimerin caused apoptosis and autophagy in K562 cells through G_1 phase arrest and produced oxidative stress-inducing JNK activation [28]. Likewise, oxidative stress induced by pristimerin was associated with JNK activation in glioma cells [29], colorectal [30] and cervical [31]. Interestingly, TG and 22-HTG caused DNA damage and MAPK-mediated apoptosis in AML cell line HL-60.

As mentioned above, previous studies using 22-HTG also observed induction of apoptosis and suppression of invasiveness of melanoma cells by inhibiting MMP-2 and MMP-9 activity and expression of BRAF, NRAS and KRAS genes [7,8]. Here, we observed that TG also reduces the expression of the cell cycle genes CDK4, CDK5 and CDK8, topoisomerases type II genes, aurora kinase C (AURKC) gene and the RAS signaling genes HRAS, KRAS and NRAS. While 22-HTG also reduces the expression of the cell cycle gene CDK8, the topoisomerase type II gene and the transcription factors genes ATF2 and HIF1A. These data indicate that cell cycle control proteins, topoisomerases, aurora kinase C, RAS signaling and transcription factors genes ATF2 and HIF1A can also be targets of TG and 22-HTG.

In summary, we showed the ability of TG and 22-HTG to inhibit the proliferation of AML cell line HL-60 cells by inducing apoptosis. Suppression of the thioredoxin system following treatment with TG and 22-HTG result in oxidative stress, leading to DNA damage and MAPK activation, which contribute to TG and 22-HTG-mediated apoptotic cell death. The molecular mechanism of action proposed for TG and 22-HTG in HL-60 cells is shown in Fig. 13.

CRediT authorship contribution statement

ACBCR: Conceptualization; Formal analysis; Investigation; Methodology. **LMB**: Investigation; Methodology. **SPN**: Investigation; Methodology. **MBPS**: Funding acquisition; Supervision; Visualization. **RBD**: Investigation; Methodology. **LFV**: Investigation; Methodology. **CAGR**: Investigation; Methodology, Funding acquisition; Supervision; Visualization. **EVC**: Investigation; Methodology. **FMAS**: Investigation; Methodology. **WCR**: Investigation; Methodology. **HHFK**: Investigation; Methodology Conceptualization; Funding acquisition; Visualization. **DPB**: Conceptualization; Formal analysis; Roles/Writing – original draft; Writing – review & editing.

Conflicts of interest

The authors have declared that there are no conflicts of interest.

Acknowledgments

The authors would like to thanks the flow cytometry core of FIOCRUZ-Bahia for flow cytometry data collection. This work was financially supported by Brazilian agencies: Coordenação de Aperfeiçoamento de Pessoal de Nível Superior (CAPES); Conselho Nacional de Desenvolvimento Científico e Tecnológico (CNPq); Fundação de Amparo à Pesquisa do Estado do Amazonas (FAPEAM); and Fundação de Amparo à Pesquisa do Estado da Bahia (FAPESB).

Appendix A. Supporting information

Supplementary data associated with this article can be found in the online version at doi:10.1016/j.biopha.2021.112034.

References

[1] H. Sung, J. Ferlay, R.L. Siegel, M. Laversanne, I. Soerjomataram, A. Jemal, F. Bray, Global cancer statistics 2020: GLOBOCAN estimates of incidence and mortality worldwide for 36 cancers in 185 countries, CA Cancer J. Clin. (2020), https://doi.org/10.3322/caac.21660.

[2] American Cancer Society. Cancer Facts & Figures 2020. Atlanta, Ga: American Cancer Society; 2020.

[3] H. Dombret, C. Gardin, An update of current treatments for adult acute myeloid leukemia, Blood 127 (1) (2016) 53–61, https://doi.org/10.1182/blood-2015-08-604520.

[4] R. Bavovada, G. Blaskó, H.L. Shieh, J.M. Pezzuto, G.A. Cordell, Spectral assignment and cytotoxicity of 22-hydroxytingenone from *Glyptopetalum sclerocarpum*, Planta Med. 56 (4) (1990) 380–382, https://doi.org/10.1055/s-2006-960988.

[5] B. Cevatemre, B. Botta, M. Mori, S. Berardozzi, C. Ingallina, E. Ulukaya, The plant-derived triterpenoid tingenin B is a potent anticancer agent due to its cytotoxic activity on cancer stem cells of breast cancer in vitro, Chem. Biol. Interact. 260 (2016) 248–255, https://doi.org/10.1016/j.cbi.2016.10.001.

[6] A.C.B.D.C. Rodrigues, F.P. Oliveira, R.B. Dias, C.B.S. Sales, C.A.G. Rocha, M.B. P. Soares, E.V. Costa, F.M.A.D. Silva, W.C. Rocha, H.H.F. Koolen, D.P. Bezerra, In vitro and in vivo anti-leukemia activity of the stem bark of *Salacia impressifolia* (Miers) A. C. Smith (Celastraceae), J. Ethnopharmacol. 1 (231) (2019) 516–524, https://doi.org/10.1016/j.jep.2018.11.008.

[7] E.S.P. Aranha, E.L. da Silva, F.P. Mesquita, L.B. de Sousa, F.M.A. da Silva, W. C. Rocha, E.S. Lima, H.H.F. Koolen, M.E.A. de Moraes, R.C. Montenegro, M.C. de Vasconcellos, 22β-hydroxytingenone reduces proliferation and invasion of human melanoma cells, Toxicol. In Vitro 66 (2020), 104879, https://doi.org/10.1016/j.tiv.2020.104879.

[8] E.S.P. Aranha, A.J.S. Portilho, L. Bentes de Sousa, E.L. da Silva, F.P. Mesquita, W. C. Rocha, F.M. Araújo da Silva, E.S. Lima, 22β-hydroxytingenone induces apoptosis

and suppresses invasiveness of melanoma cells by inhibiting MMP-9 activity and MAPK signaling, J. Ethnopharmacol. 267 (2021), 113605, https://doi.org/10.1016/j.jep.2020.113605.
[9] H. Morita, Y. Hirasawa, A. Muto, T. Yoshida, S. Sekita, O. Shirota, Antimitotic quinoid triterpenes from Maytenus chuchuhuasca, Bioorg. Med. Chem. Lett. 18 (3) (2008) 1050–1052, https://doi.org/10.1016/j.bmcl.2007.12.016.
[10] T.H. Desai, S.V. Joshi, In silico evaluation of apoptogenic potential and toxicological profile of triterpenoids, Indian J. Pharmacol. 51 (3) (2019) 181–207, https://doi.org/10.4103/ijp.IJP_90_18.
[11] S.A. Ahmed, R.M.Jr Gogal, J.E. Walsh, A new rapid and simple non-radioactive assay to monitor and determine the proliferation of lymphocytes: an alternative to [^{3}H]thymidine incorporation assay, J. Immunol. Methods 170 (1994) 211–224.
[12] L.S. Santos, V.R. Silva, L.R.A. Menezes, M.B.P. Soares, E.V. Costa, D.P. Bezerra, Xylopine induces oxidative stress and causes G_2/M Phase arrest, triggering caspase-mediated apoptosis by p53-independent pathway in HCT116 cells, Oxid. Med. Cell. Longev. 2017 (2017), 7126872.
[13] V.R. Silva, R.S. Corrêa, L.S. Santos, M.B.P. Soares, A.A. Batista, D.P. Bezerra, A ruthenium-based 5-fluorouracil complex with enhanced cytotoxicity and apoptosis induction action in HCT116 cells, Sci. Rep. 8 (1) (2018) 288.
[14] I. Nicoletti, G. Migliorati, M.C. Pagliacci, F. Grignani, C. Riccardi, A rapid and simple method for measuring thymocyte apoptosis by propidium iodide staining and flow cytometry, J. Immunol. Methods 139 (1991) 271–279.
[15] F.X. Sureda, E. Escubedo, C. Gabriel, J. Comas, J. Camarasa, A. Camins, Mitochondrial membrane potential measurement in rat cerebellar neurons by flow cytometry, Cytometry 28 (1997) 74–80.
[16] K.J. Livak, T.D. Schmittgen, Analysis of relative gene expression data using real-time quantitative PCR and the 2(-Delta Delta C(T)) Method, Methods 25 (2001) 402–408.
[17] L.S. Glass, A. Bapat, M.R. Kelley, M.M. Georgiadis, E.C. Long, Semi-automated high-throughput fluorescent intercalator displacement-based discovery of cytotoxic DNA binding agents from a large compound library, Bioorg. Med. Chem. Lett. 20 (2010) 1685–1688.
[18] D. Hanahan, R.A. Weinberg, Hallmarks of cancer: the next generation, Cell 144 (2011) 646–674.
[19] L. Shao, M.B. Diccianni, T. Tanaka, R. Gribi, A.L. Yu, J.D. Pullen, B.M. Camitta, J. Yu, Thioredoxin expression in primary T-cell acute lymphoblastic leukemia and its therapeutic implication, Cancer Res. 61 (19) (2001) 7333–7338.
[20] H. Li, M. Li, G. Wang, F. Shao, W. Chen, C. Xia, S. Wang, Y. Li, G. Zhou, Z. Liu, EM23, a natural sesquiterpene lactone from *Elephantopus mollis*, induces apoptosis in human myeloid leukemia cells through thioredoxin- and reactive oxygen species mediated signaling pathways, Front. Pharmacol. 7 (2016) 77, https://doi.org/10.3389/fphar.2016.00077.
[21] Z. Zheng, S. Fan, J. Zheng, W. Huang, C. Gasparetto, N.J. Chao, J. Hu, Y. Kang, Inhibition of thioredoxin activates mitophagy and overcomes adaptive bortezomib resistance in multiple myeloma, J. Hematol. Oncol. 11 (2018) 29, https://doi.org/10.1186/s13045-018-0575-7.
[22] W. Xie, W. Ma, P. Liu, F. Zhou, Overview of thioredoxin system and targeted therapies for acute leukemia, Mitochondrion 47 (2019) 38–46, https://doi.org/10.1016/j.mito.2019.04.010.
[23] J.J. Jia, W.S. Geng, Z.Q. Wang, L. Chen, X.S. Zeng, The role of thioredoxin system in cancer: strategy for cancer therapy, Cancer Chemother. Pharmacol. 84 (2019) 453–470, https://doi.org/10.1007/s00280-019-03869-4.
[24] E. Clapper, S. Wang, P.V. Raninga, G. Di Trapani, K.F. Tonissen, Cross-talk between Bcr-abl and the thioredoxin system in chronic myeloid leukaemia: implications for CML treatment, Antioxidants 9 (2020) 207, https://doi.org/10.3390/antiox9030207.
[25] G.J. Samaranayake, C.I. Troccoli, M. Huynh, R. Lyles, K. Kage, A. Win, V. Lakshmanan, D. Kwon, Y. Ban, S.X. Chen, E.R. Zarco, M. Jorda, K.L. Burnstein, P. Rai, Thioredoxin-1 protects against androgen receptor-induced redox vulnerability in castration-resistant prostate cancer, Nat. Commun. 8 (2017) 1204, https://doi.org/10.1038/s41467-017-01269-x.
[26] R.R. Singh, J. Mohammad, M. Orr, K.M. Reindl, Glutathione S-transferase pi-1 knockdown reduces pancreatic ductal adenocarcinoma growth by activating oxidative stress response pathways, Cancers 12 (2020) 1501, https://doi.org/10.3390/cancers12061501.
[27] Q. Zhao, Y. Liu, J. Zhong, Y. Bi, Y. Liu, Z. Ren, X. Li, J. Jia, M. Yu, X. Yu, Pristimerin induces apoptosis and autophagy via activation of ROS/ASK1/JNK pathway in human breast cancer in vitro and in vivo, Cell Death Discov. 5 (2019) 125, https://doi.org/10.1038/s41420-019-0208-0.
[28] Y. Liu, Z. Ren, X. Li, J. Zhong, Y. Bi, R. Li, Q. Zhao, X. Yu, Pristimerin Induces autophagy-mediated cell death in K562 cells through the ROS/JNK signaling pathway, Chem. Biodivers. 16 (8) (2019), 1900325, https://doi.org/10.1002/cbdv.201900325.
[29] H. Zhao, C. Wang, B. Lu, Z. Zhou, Y. Jin, Z. Wang, L. Zheng, K. Liu, T. Luo, D. Zhu, G. Chi, Y. Luo, P. Ge, Pristimerin triggers AIF-dependent programmed necrosis in glioma cells via activation of JNK, Cancer Lett. 374 (1) (2016) 136–148, https://doi.org/10.1016/j.canlet.2016.01.055.
[30] Q. Zhao, Y. Bi, J. Guo, Y. Liu, J. Zhong, Y. Liu, L. Pan, Y. Guo, Y. Tan, X. Yu, Effect of pristimerin on apoptosis through activation of ROS/ endoplasmic reticulum (ER) stress-mediated noxa in colorectal cancer, Phytomedicine 80 (2021), 153399, https://doi.org/10.1016/j.phymed.2020.153399.
[31] J.Y. Byun, M.J. Kim, D.Y. Eum, C.H. Yoon, W.D. Seo, K.H. Park, J.W. Hyun, Y. S. Lee, J.S. Lee, M.Y. Yoon, S.J. Lee, Reactive oxygen species-dependent activation of Bax and poly(ADP-ribose) polymerase-1 is required for mitochondrial cell death induced by triterpenoid pristimerin in human cervical cancer cells, Mol. Pharmacol. 76 (4) (2009) 734–744, https://doi.org/10.1124/mol.109.056259.